Selecting for Surface-Induced vs. Bulk Crystallization in P3HT Thin Films:

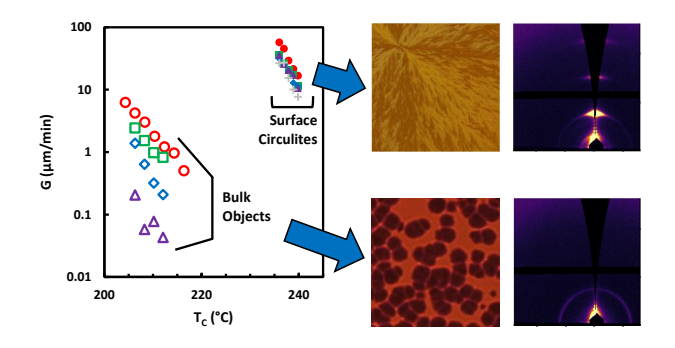
Distinct Morphology, Orientation, and Linear Growth Rates

Jesse Kuebler¹, Sunil Dhapola¹, Lucia Fernandez-Ballester^{1*}

¹Department of Mechanical and Materials Engineering and Nebraska Center for Materials and Nanoscience, University of Nebraska at Lincoln, Lincoln, Nebraska 68588, United States.

*Corresponding author: Email: lucia.fernandez@unl.edu

For Table of Contents use only



Keywords: conjugated polymers, crystallization, interfacial effects, linear growth-rate, thin films

Abstract

By removing the air-polymer interface in poly(3-hexylthiopene) (P3HT) thin films, bulk crystallization morphology is attained, where highly absorbing "bulk objects" grow throughout the film thickness at T \sim T_{C,BULK} and exhibit no preferential crystalline orientation. In contrast, films with a free surface develop highly edge-on oriented 2D spherulites ("circulites") at the air-polymer interface at T >> T_{C,BULK}, which then promote edge-on oriented, featureless crystallization in the underlayer near T_{C,BULK}. Interestingly, circulites exhibit ~10x faster linear growth rates than bulk objects—despite both morphologies consisting

of the same crystal form—at temperatures where chain mobility is not expected to dominate growth rates, suggesting that another mechanism may be at play. Overall, these results provide insight into the role of the free surface in the crystallization process and indicate that the presence/absence of an air-polymer interface can be used to control semicrystalline morphology and orientation of P3HT thin films.

1. Introduction

In the search for improved organic electronic devices, conjugated polymers are an attractive option due to their low weight, intrinsic flexibility, and potential to manipulate final properties through molecular characteristics and processing pathways. In P3HT—a model semicrystalline conjugated polymer molecular weight, regioregularity, and processing conditions such as thermal history and solvent evaporation rates can significantly impact crystallization kinetics and final semicrystalline morphology.¹⁻⁹ Solution processing is typically used in conjugated thin films relevant to electronic applications because it is fast and inexpensive, but it often involves ill-defined conditions that make it difficult to control the crystallization process. Melt processing, however, enables facile control over crystallization conditions and may result in morphologies not achievable in the presence of solvents, but is not yet fully understood. In particular, the potential to optimize morphology and properties in melt-crystallized conjugated polymer thin films remains largely untapped, partly due to the difficulty of probing the crystallization process in thin films. In general, the crystallization behavior in polymer thin films can deviate from that in the bulk due to the possibility of confinement effects and of substrate or air-polymer interfacial effects, 10-16 and the exact effect that the substrate and air interfaces have on polymer crystallization depend on the specific polymer and substrate interactions. 17-19 Furthermore, whether the presence or absence of an airpolymer interface in a thin film can be used to manipulate the type and orientation of semicrystalline morphologies in conjugated polymers remains undetermined.

The critical role that the air-polymer interface can play on P3HT crystallization has recently been observed. Our group provided direct evidence of free surface-induced crystallization: distinct, highly edge-on oriented, 2-dimensional spherulite-like structures ("circulites") nucleated and grew laterally within 20 nm of the air-polymer interface at \sim 25 °C higher than the bulk crystallization temperature ($T_{C,BULK}$). 20 This free surface-induced crystallization was attributed to surface freezing, a relatively uncommon phenomenon thought to result from a reduced surface energy γ in the surface-frozen state ($\gamma_{cry,alir} + \gamma_{cry,liq}$) as compared to the molten state ($\gamma_{liq,alir}$). $^{21-25}$ While most materials exhibit decreased melting or glass transition temperatures at the free surface compared to the bulk—ascribed to increased molecular mobility at the surface $^{26-30}$ —surface freezing results in higher crystallization or melting temperatures at the free surface and has been reported for a few materials such as linear alkanes, poly (n-alkyl acrylates), and alcohols. $^{21-22,31-32}$

Surface freezing is still not fully understood and, in particular, little is known about how surface freezing impacts the nucleation and growth processes compared to crystallization in the bulk. Typically, studies on surface freezing report the transition temperature, thickness, and crystal structure of the surface frozen layer, but not the corresponding nucleation or crystalline growth rates. In the case of P3HT, there are extremely few reports of nucleation and growth rates during melt-crystallization. P3HT is thought to typically exhibit high nucleation densities, $^{33-34}$ which may partly explain the small number of examples in literature of individual, optically resolvable melt-crystallized morphologies suitable for crystalline growth rate measurements. $^{20, 33, 35}$ Many studies of bulk P3HT crystallization use techniques such as calorimetry and X-ray diffraction, which do not yield nucleation or growth rates. $^{1, 36-37}$ Using optical microscopy, Koch *et al.* reported $^{\sim}60 \,\mu\text{m}/\text{min}$ growth rate for form I spherulites in a low molecular weight P3HT (below the chain-folding limit of $M_n \sim 5.5 \,\text{kDa}$) using films with a free surface. $^{33, 38-39}$ Our group previously observed nucleation and growth of circulites at the air-polymer interface; however, the crystallization at bulk-like temperatures of the remainder of the film resulted in featureless morphology

under the optical microscope, so underlayer growth rates could not be extracted and a comparison to surface-induced growth rates could not be established.²⁰ Furthermore, the bulk-like underlayer was thought to be nucleated by the free surface-induced circulite layer, so it is uncertain whether it corresponded to the same type of morphology that arises during crystallization of bulk P3HT.

In this work, we attain the bulk P3HT morphology in 40 to 200 nm covered thin films—analogous to the morphology in ~ 10 µm thick films—where individual nucleation and growth of "bulk objects" ("BOs") can be directly observed. The comparison of morphology and linear growth rates of surface-induced "circulites" (in uncovered films) vs. BOs (in covered films) provides insight on the impact of the air-polymer interface on the melt-crystallization process. Unexpectedly, the linear growth rate of circulites is at least one order of magnitude larger than that of BOs—even though circulites exhibit the same crystalline structure as BOs and crystallize at temperatures ≥ 25 °C higher, where chain mobility is not expected to dominate growth rates. We also show that a melt-crystallized covered thin film exhibits isotropic orientation—in contrast to the strong edge-on orientation in melt-crystallized uncovered thin films—and that the free exciton bandwidth of films during growth of BOs is significantly larger than that of circulites. The results here provide fundamental knowledge on the role of the air-polymer interface on melt crystallization and indicate that the presence or absence of a free surface during melt-crystallization can be used to manipulate overall semicrystalline morphology and orientation of P3HT thin films.

2. Experimental

2.1. Materials

Poly(3-hexylthiophene) (P3HT) with 95% regionegularity, weight-averaged molecular weight of 40 kg/mol, and polydispersity index of 2.1 was purchased from Rieke Metals and used as received.

2.2. Sample preparation

P3HT solutions in o-dichlorobenzene (Sigma Aldrich) with concentrations between 8 and 30 mg/mL were prepared by stirring at 80 °C for ~24 h in argon atmosphere. Prior to spin coating or drop casting, the solutions were heated to 80 °C for 10 min. Thin films (≤ 200 nm) were spin coated (SC) on cleaned glass coverslips or 18 mm x 18 mm silicon wafers with 285 nm thermal oxide layer (University Wafer). Covered films for optical measurements were prepared under argon atmosphere by heating a SC film to 280 °C and pressing a small piece of glass into the molten film. Covered films for Grazing Incidence Wide-Angle X-ray Scattering (GIWAXS) were prepared by thermally evaporating aluminum onto a SC film. Thick films (~10 μm) for optical experiments were prepared by melting P3HT powder between two glass coverslips at 280 °C under argon atmosphere. Uncovered thick films were obtained by peeling apart the two glass coverslips of a prepared thick film while the polymer was fully molten. A bulk sample (~100 μm) for transmission X-ray experiments was prepared by drop casting 0.1 mL of 30 mg/mL solution onto aluminum foil. A second piece of foil was placed on top, and the resulting packet was sealed using Kapton tape. A Keyence VK-X200K laser scanning microscope was used to measure the thickness of thin films.

2.3. Characterization

Optical micrographs and UV-vis spectra were collected and analyzed as detailed elsewhere.²⁰ In short, the micrographs and spectra were collected simultaneously while heating and cooling at 10 °C/min. Flowing nitrogen gas and a homemade shutter were used to minimize sample degradation. Absorbance spectra were averaged between 570 and 640 nm, and the numerical derivative with respect to temperature was calculated to track the crystallization process. To extract the free exciton bandwidth, the spectra were fitted using equation 1

$$A(E) \propto \sum_{m=0}^{\infty} \left(\frac{S^m}{m!}\right) \left(1 - \frac{We^{-S}}{2E_p} \sum_{n \neq m} \frac{S^n}{n!(n-m)}\right)^2 exp\left(-\frac{\left(E - E_0 - mE_p - \frac{1}{2}WS^me^{-S}\right)^2}{2\sigma^2}\right) \qquad \qquad \textit{Equation 1}$$

where A(E) is the absorbance spectrum, S is the Huang-Rhys parameter of disordered chains (S = 1.1), and E_P is the vibrational energy of the effective carbon-stretching mode (E_P = 175 meV). The fitting parameters are the free exciton bandwidth (W), the transition energy of the A_{0-0} peak (E_0), and the Gaussian linewidth (σ). $^{40-41}$

Isothermal growth rates were calculated from real-time optical micrographs by measuring the diameter along two perpendicular directions of an object before impingement using ImageJ software. The growth rate was taken as one half of the slope of the best fit line of diameter vs. time. The growth rate of at least 3 objects was measured for each temperature. Although nucleation and growth of circulites is observed up to $T_{iso} = 243.5$ °C, isothermal growth rates could not be accurately measured for $T_{iso} > 240$ °C (Figure S1 in Supporting Data). The melting endset temperature ($T_{M,END}$) was determined by heating an isothermally crystallized film at 2 °C/min to minimize superheating. Nucleation density was determined by counting the number of objects in a given area and normalizing by the layer thickness. Self-nucleation experiments were performed by fully melting the film, cooling to 100 °C at 10 °C/min, heating to the seeding temperature (T_{s}) at 10 °C/min, holding isothermally for 5 minutes, and then cooling at 10 °C/min while acquiring micrographs and UV-vis spectra.

GIWAXS patterns were collected at the 8-ID-E beamline (Advanced Photon Source, Argonne National Laboratory)⁴³ with 10.92 keV incident X-rays defined by 200 μ m x 10 μ m (H x V) slits. A Pilatus 1 M detector positioned 217 mm from the sample was used to collect two-dimensional (2D) diffraction patterns (0.172 mm × 0.172 mm pixel size), which were corrected for geometry and remapped using the GIXSGUI MATLAB package.⁴⁴ Transmission wide angle X-ray scattering (WAXS) patterns of bulk samples were acquired at the 12-ID-B beamline (Advanced Photon Source, Argonne National Laboratory), using 13.30 keV incident X-rays and a Pilatus 300k 2D detector mounted 0.4 m from the sample. The 1D intensity (I) vs. scattering vector (q) plots were calculated by radially averaging the 2D patterns.

3. Results

3.1. Bulk crystallization and morphology in thin films

Upon cooling bulk covered samples (~10 μm thick) from the molten state, nucleation and growth of round, highly absorbing objects—referred to as "bulk objects" or "BOs"—are observed in optical micrographs (Figure 1a). At the same time, an increase in UV-vis absorbance—corresponding to a peak in the absorbance derivative—is observed during crystallization at T_{C,BULK} ~201 °C (Figure 1b). Interestingly, similar morphologies are clearly observed during the crystallization event at ~199 °C of a ~200 nm covered thin film, suggesting that the bulk objects can also develop in thin films without an air-polymer interface. In contrast, uncovered 200 nm films with an air-polymer interface exhibit an additional peak at ~232 °C—corresponding to spherulitic crystallization confined within 20 nm of the free surface²⁰ (Figure 2a), referred to as "circulites"—while the remainder of the film ("underlayer") crystallizes at ~205 °C but no individual morphologies can be optically resolved (Figure 1).

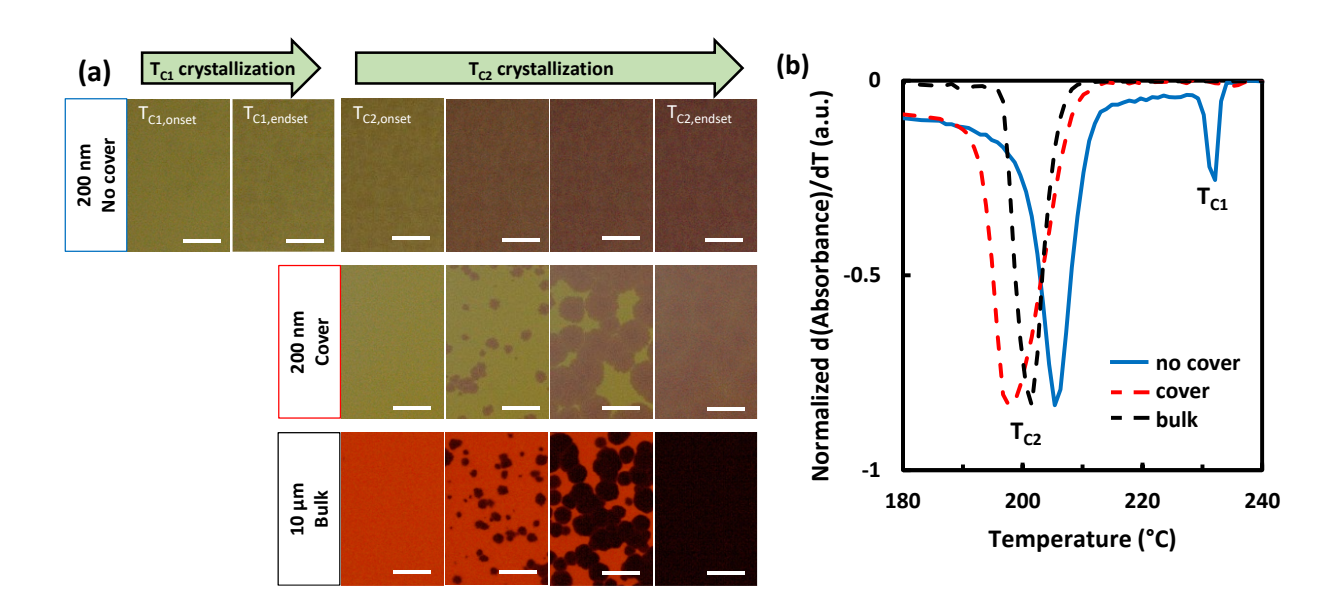


Figure 1. (a) Transmission micrographs during non-isothermal crystallization of covered and uncovered 200 nm thin films and covered 10 μ m bulk films. Scalebar is 30 μ m. (b) Normalized absorbance derivatives during crystallization.

Unlike circulites at the air-polymer interface of the uncovered film, bulk objects in covered films do not exhibit the characteristic Maltese cross under crossed polars (Figure 2a). Note that the size at impingement of BOs is similar to that of circulites ($^{\sim}10-30~\mu m$), but large-scale birefringence is not apparent in the bulk objects. Correspondingly, the polarized reflectance does not increase during crystallization of bulk objects at $^{\sim}201~^{\circ}$ C, unlike during crystallization of the circulites at $^{\sim}232~^{\circ}$ C: under crossed polars, the BO derivative peak is negative, and the surrounding melt is brighter than the BOs, suggesting that the growing crystals' absorption is stronger than their reflected, phase retarded intensity (Figure 2b).

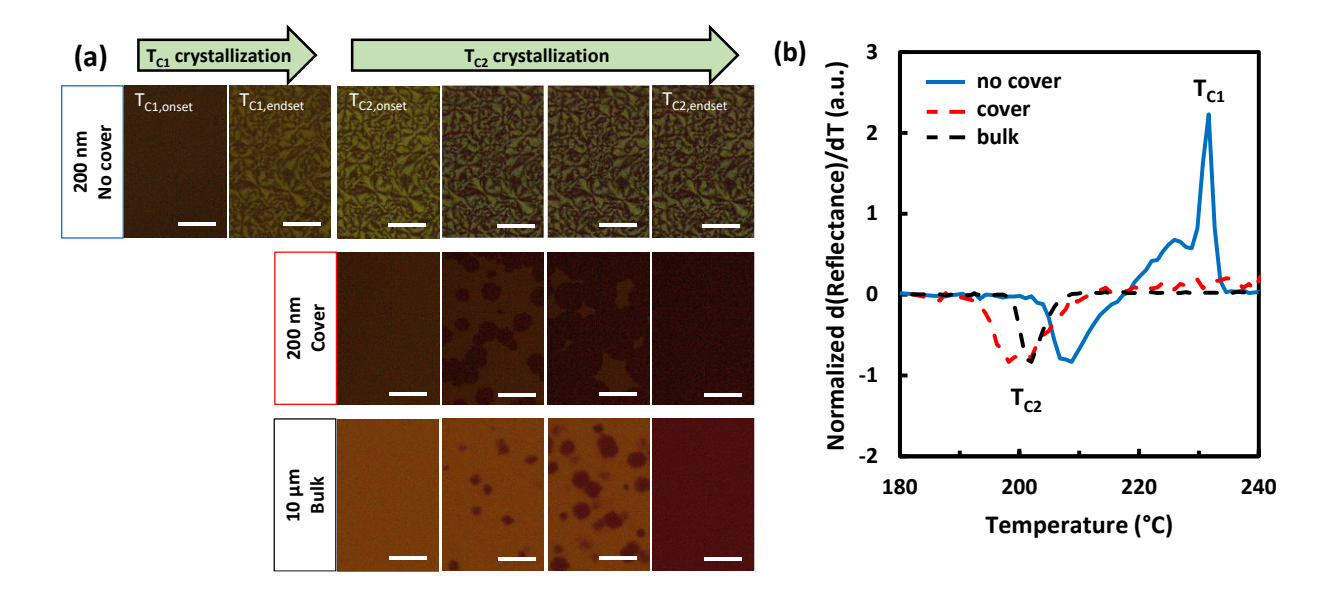


Figure 2. (a) Polarized reflection micrographs during non-isothermal crystallization of 200 nm thin films and covered 10 μ m bulk films. Scalebar is 30 μ m. (b) Normalized polarized reflection derivatives during crystallization.

Although the bulk objects do not have a Maltese cross, they do exhibit very faint, small birefringent grains without any apparent correlation to the overall shape of the bulk object (i.e. the grains appear to be randomly distributed within the objects) (Figure 3b and c) despite the radial growth of BOs. The birefringent grains are only visible when absorbance is minimized by covering a very thin film (40 nm), the bulk object size is maximized (~20 µm diameter) using isothermal crystallization, and the camera integration time is increased by 2.5 times (compared to Figure 3a). In contrast, circulites of a similar size exhibit strong, long-range, radially symmetric birefringence resulting in a Maltese cross (Figure 3a). Such difference indicates that the bulk objects and circulites are organized somewhat differently at the mesoscale.

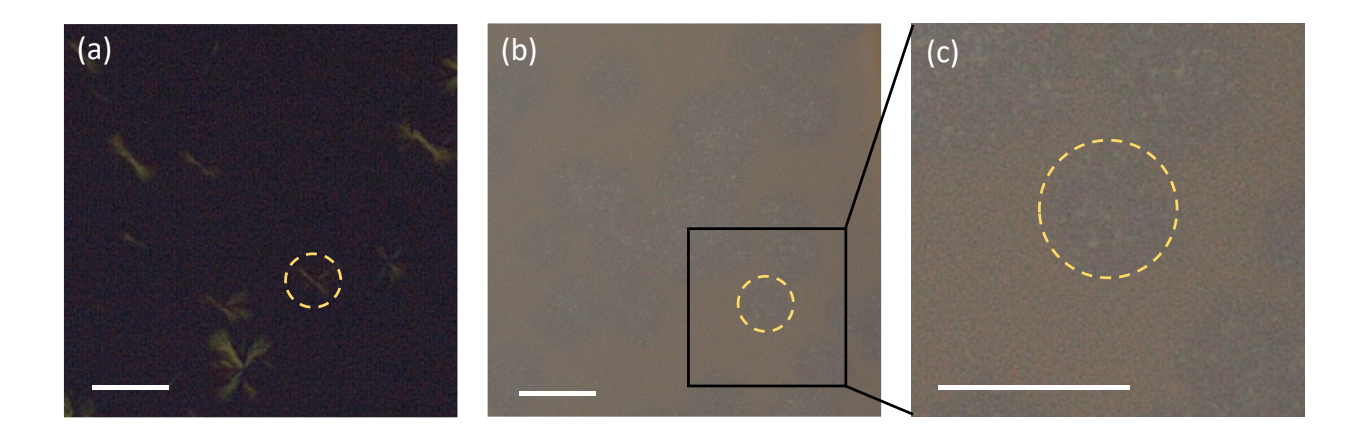


Figure 3. Polarized reflection micrographs of (a) circulites and (b, c) BOs formed in 40 nm thick films. Dashed circles serve to guide the eye to similarly sized objects. Camera exposure time is 100 ms for BOs, but 40 ms for circulites. Scalebar is 30 μ m.

To determine whether the bulk objects grow throughout the thickness t of the film or are confined within a specific layer (like the circulites are confined at the free surface), the area under each crystallization peak in the UV-vis absorbance derivative (Figure 4) was quantified for films of various thicknesses ranging from 40 nm to 10 μ m. In covered films, the BO crystallization peak area increases

monotonously with t indicating that bulk objects pervade the entire film thickness (Figure 5a). In uncovered films, the circulite peak area is nearly constant with t and indicates fixed thickness of the circulite layer even for $t \sim 10 \, \mu m$, whereas the increase of the underlayer peak area implies that crystallization of the featureless underlayer pervades the remaining film thickness. Overall, the results indicate that, unlike the 2-dimensional circulites, bulk objects grow in 3-dimensions until they impinge (with other BOs, the substrate interface, or the top cover).

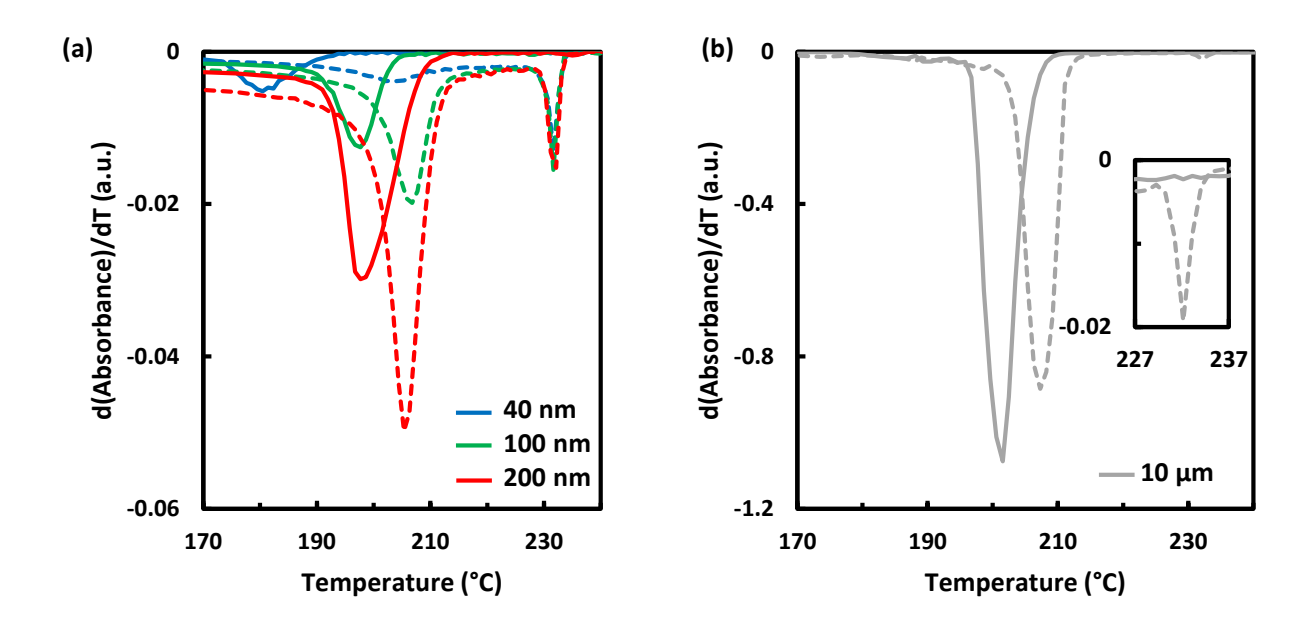


Figure 4. Absorbance derivatives during non-isothermal crystallization of (a) $^{\sim}200$ nm, 100 nm, 40 nm, and (b) 10 μ m films with free (dashed) and covered (solid) surfaces. Inset in (b) shows zoomed-in circulite crystallization peak.

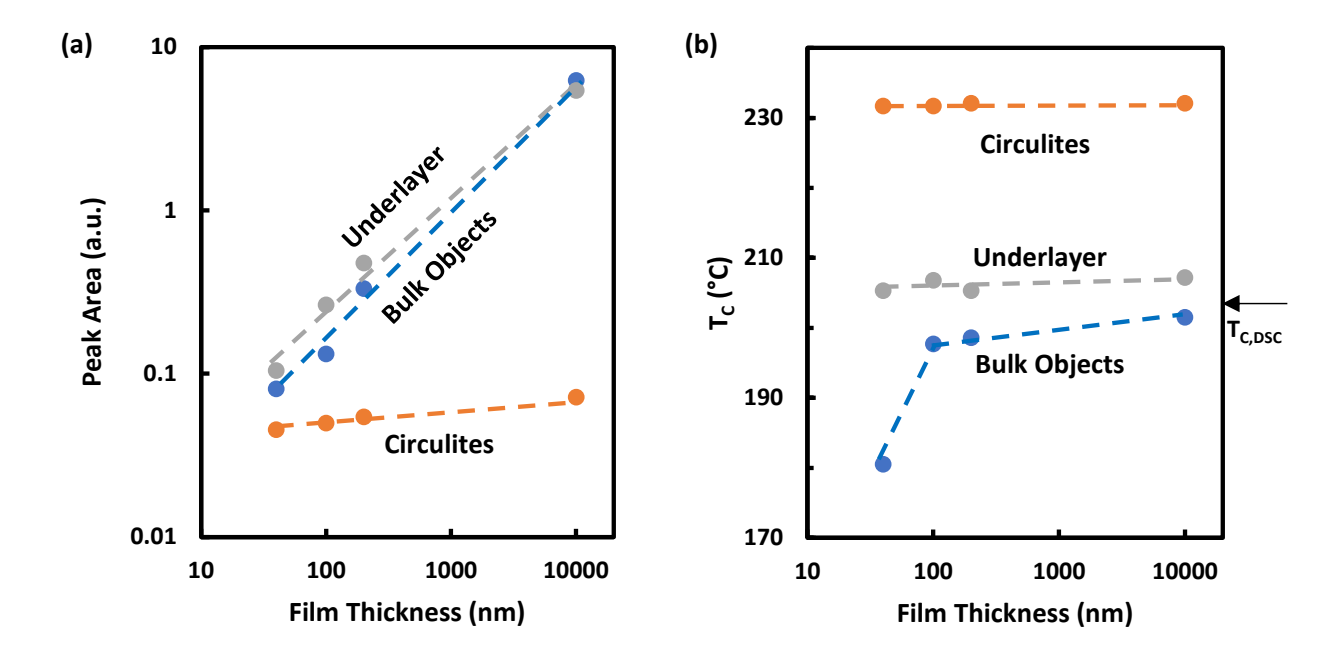


Figure 5. (a) Integrated area under absorbance derivative crystallization peaks for films of different thicknesses. (b) Crystallization temperature vs. film thickness t; the arrow represents the DSC bulk crystallization temperature.²⁰ Dashed lines are guidelines.

Interestingly, the crystallization temperatures do not vary with thickness t except for BO crystallization in the thinnest film (i.e. 40 nm), which is depressed by nearly 20 °C compared to thicker films between 100 nm - 10 μ m and to the bulk DSC crystallization temperature (Figure 5b). Such decrease may be attributed to kinetic hindering of crystallization—possibly due to substrate interactions or confinement effects that impede nucleation and/or growth. It should be noted that the reduced crystallization temperature does not correlate with a decrease in the extent of BO crystallization in the 40 nm covered film; that is, the area of the BO crystallization peak does not deviate from the trend with t (Figure 5a). For uncovered films, however, it is interesting to note that no decrease in T_C of the featureless underlayer is observed for 40 nm films indicating that, unlike for BOs, overall crystallization kinetics of the featureless underlayer are not significantly hindered by confinement or substrate effects. In the case of circulites, the

invariability of crystallization temperature with t is expected, since it has been previously shown that circulites always grow confined within 20 nm of the free surface so they experience the same confinement for all t > 20 nm.²⁰

3.2. Free surface vs. bulk linear growth rates

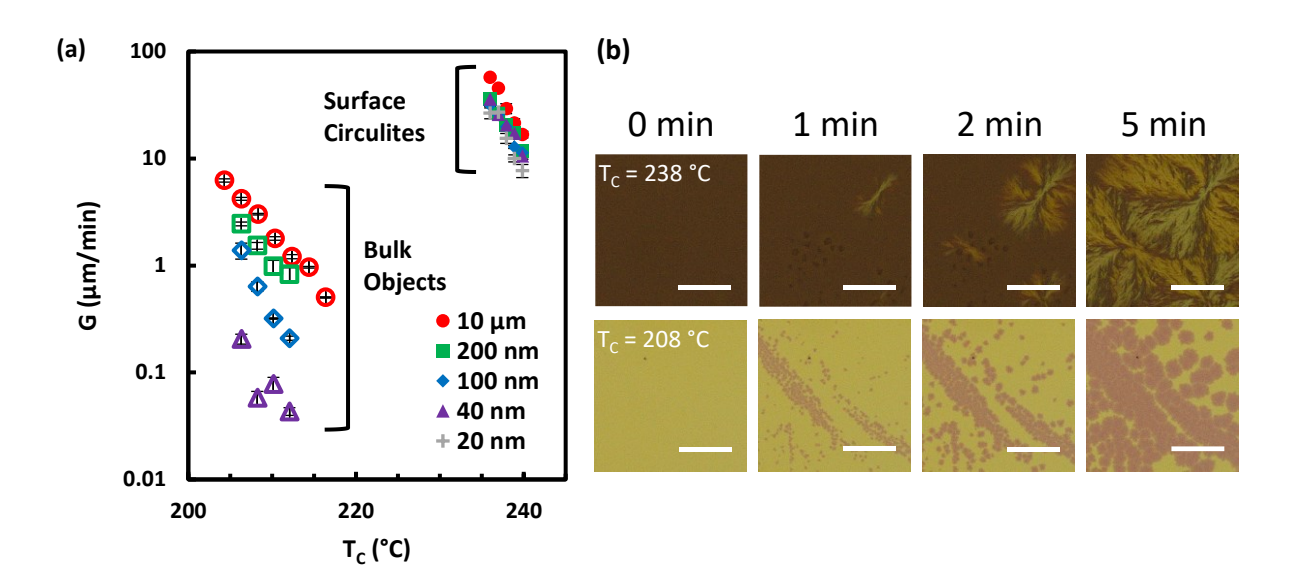


Figure 6. (a) Isothermal linear growth rates G of bulk objects (open shapes) and circulites (filled shapes) in P3HT films with thickness of 10 μ m (red circles), 200 nm (green squares), 100 nm (blue diamonds), 40 nm (purple triangles), and 20 nm (grey crosses). (b) Representative polarized reflection (top) and transmission (bottom) optical micrographs taken during isothermal crystallization of a 200 nm film. Scalebar is 50 μ m.

Linear growth rates G were measured under isothermal conditions for both free surface circulites in uncovered films and bulk objects in covered films, and clearly show that circulites grow approximately one order of magnitude faster than bulk objects despite their \sim 25 °C higher crystallization temperature (Figure 6a). In fact, extrapolation of $G_{BULK\ OBJECTS}$ suggests that, at the crystallization temperature of circulites, BOs would exhibit growth rates at least three orders of magnitude slower than $G_{CIRCULITES}$. For both morphologies, G increases with decreasing T_{C_r} as expected for crystallization temperatures close to

the melting point where crystallization kinetics are dominated by thermodynamic effects, not chain mobility effects. Therefore, the faster growth rate of circulites compared to BOs is surprising: clearly, the presence of an air-polymer interface affects G, but the underlying mechanism is unknown. It is important to note that the crystalline structure of the BOs and circulites is the same and corresponds to form I of P3HT (section 3.3), so the vast difference in growth rate of circulites and bulk objects cannot be attributed to a polymorphic difference.

The effect of film thickness on G is consistent with the T_C vs. t trends in Figure 5b: G is nearly unaffected by film thickness except for bulk objects in the thinnest films (Figure 6a). Indeed, $G_{BULK\ OBJECTS}$ in 200 nm and 10 μ m films is very similar—despite the large difference in film thickness—indicating that substrate effects are negligible at 200 nm thickness and that the large discrepancy between $G_{CIRCULITES}$ and $G_{BULK\ OBJECTS}$ reflects a difference in crystallization kinetics between the free surface and the bulk phase. In contrast, $G_{BULK\ OBJECTS}$ is about one order of magnitude smaller in the 40 nm film than in films 200 nm or thicker: bulk object crystallization is likely slowed down by substrate interactions in the thinnest films. Interestingly, $G_{CIRCULITES}$ is nearly unaffected by overall film thickness for 20 nm $\leq t \leq$ 10 μ m, indicating that the substrate effects that slow down the growth rate of BOs do not affect circulites in the same way.

The nucleation density during isothermal crystallization was also estimated for both circulites and bulk objects by counting their number and normalizing by the appropriate thickness (i.e. 20 nm for circulites and the entire film thickness for BOs). Representative images in Figure 6b and Figure S2 in Supporting Data indicate that the nucleation density of circulites is ~one order of magnitude lower than for BOs in films with $t \le 200$ nm (~0.001 – 0.04 nuclei/ μ m³ for circulites vs. ~0.02 – 0.5 nuclei/ μ m³ for BOs); this indicates that the much larger linear growth rates of circulites are the main contributor to the enhanced crystallization rate at the free surface. Interestingly, 10 μ m films have a circulite nucleation density similar to that of thin films, whereas the BO nucleation density is ~ 5 x 10^{-4} nuclei/ μ m³, which is significantly

smaller than in thin films and suggests that BOs may preferentially nucleate near the substrate and the top cover.

3.3. Crystalline structure and orientation

Grazing incidence wide angle X-ray scattering (GIWAXS) was performed to compare the crystalline structure and orientation of circulites (in uncovered thin films) and of bulk objects (in covered thin films). Because bulk objects are only observed in covered thin films, and GIWAXS is typically performed in thin films with a free surface, a special sample preparation procedure was carried out to attain GIWAXS patterns corresponding to bulk objects. First, a ~100 nm film was melt-crystallized to form a circulite layer at the free surface; then, a ~15 nm aluminum layer was deposited before a second melt-crystallizing (MC) cycle was carried out to form the BO morphology (Figure 7a). Note that the circulite structures remain after Al deposition: the aluminum layer is thin enough to be optically semitransparent, which allows observation of the circulites Maltese cross (Figure 7c). Furthermore, upon melt crystallization of the coated film, the optical micrographs only exhibit growth of bulk objects (Figure 7d), demonstrating that the Al layer is effective as a thin film cover.

The GIWAXS patterns revealed that both bulk objects and circulites have the same crystalline structure, and that bulk objects exhibit isotropic orientation—unlike the circulite layer which is highly edge-on oriented (Figure 7e vs. g). In the case of the Al coated films, an incident angle greater than the critical angle for aluminum ($\alpha_i > \alpha_{\text{C-Al}} \sim 0.18^{\circ}$) was employed, so that the X-rays penetrated the thin Al coating and scattering arose from the entire polymer film. The resulting GIWAXS pattern shows that BOs have (100) diffraction at $q \sim 0.38$ ($d \sim 1.6$ nm, corresponding to P3HT form I) with no preferential orientation (Figure 7g and Figure S3a). Note that transmission X-ray diffraction of a bulk film ~100 μ m thick also exhibits form I crystal structure (Figure S3c), and that covered 40 nm films show results similar

to the 100 nm film—indicating that bulk isotropic crystallites can form even in very thin films (Figure S3d,e).

In free surface films, GIWAXS patterns for α_i below and above the critical angle of P3HT ($\alpha_{\text{C-P3HT}} \sim 0.12^{\circ}$) correspond to scattering from only the top $\sim 10 \text{ nm}^{45}$ (i.e. only circulites) and from the entire film (circulites + underlayer) respectively (Figure 7e), and show that both the circulites and underlayer crystallize with form I and strong edge-on orientation. Neither circulites nor bulk objects exhibit evidence for the other known P3HT crystal structure (form II, with (100) diffraction at $q \sim 0.52 \text{ Å}^{-1}$ and $d \sim 1.2 \text{ nm}$);^{33, 46-49} therefore, both free surface-induced and bulk crystallization in thin films occur with the same crystallographic form.

It is worth pointing out that, upon coating a film with circulites already formed, GIWAXS patterns show that the film still maintains strong edge-on crystalline orientation (Figure 7f). This indicates that, in applications requiring a covered interface of the active layer, both surface-induced edge-on orientation and bulk isotropic orientation can be achieved by melt-crystallizing before or after deposition of a coating.

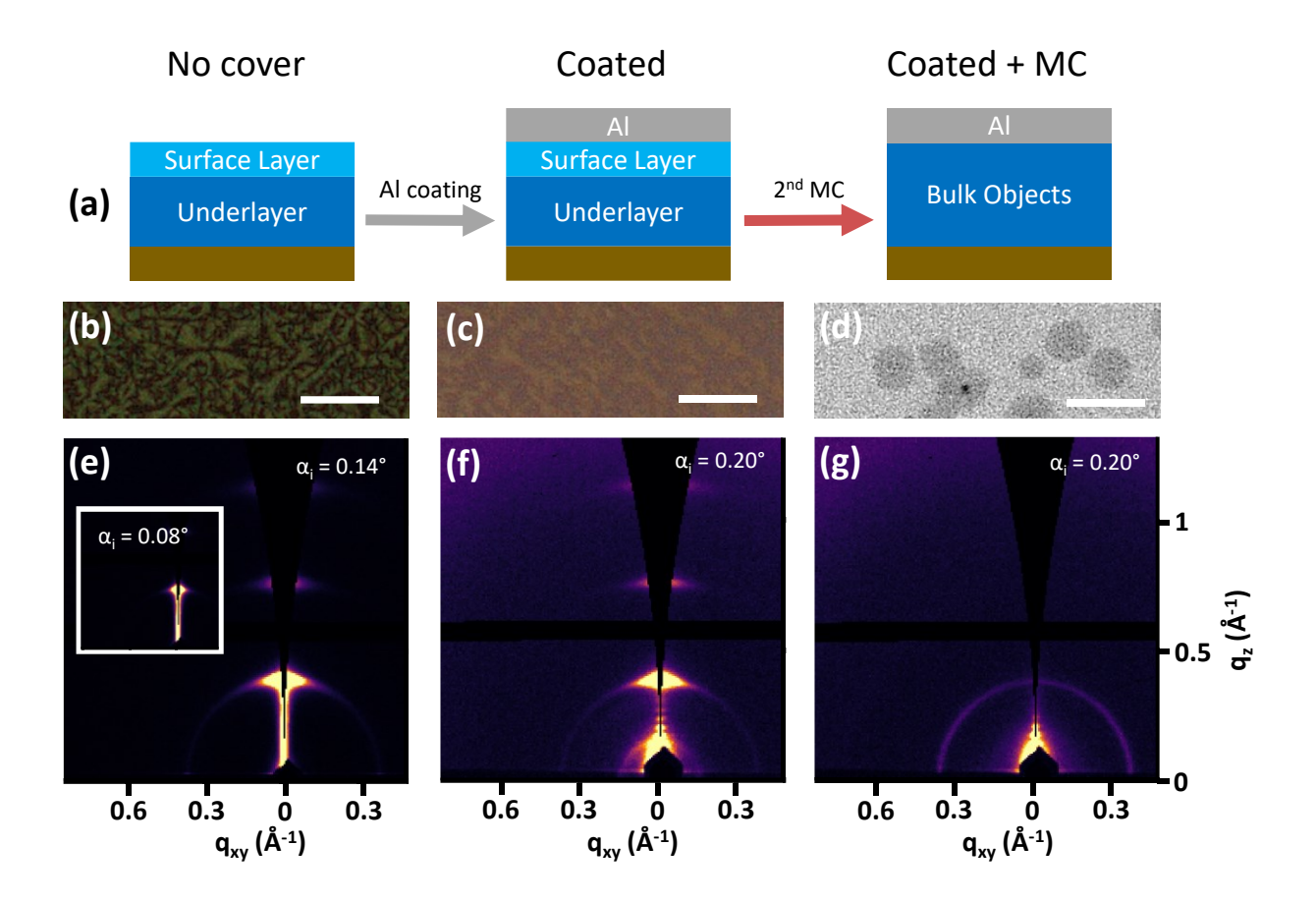


Figure 7. (a) Schematic outlining sample preparation of a melt-crystallized ~100 nm thick uncovered film, Al coated film, and Al coated + melt-crystallized (MC) film. Ex-situ polarized reflection optical micrographs of (b) uncovered and (c) Al coated films. (d) Transmission optical micrograph during crystallization of an Al coated film (green channel only, optimized brightness and contrast). Scalebar is 30 μ m. GIWAXS patterns of (e) uncovered, (f) Al coated, and (g) Al coated + MC 100 nm films.

3.4. Optical properties of free surface and bulk

The free exciton bandwidth (W) extracted from UV-vis spectra reveals that the presence or absence of an air-polymer interface during melt-crystallization significantly impacts conjugation length, given that W and conjugation length are inversely related.^{41, 50} For fully solidified uncovered films, W increases strongly with film thickness t (~50 meV for t ~ 40 nm to ~100 meV for t ~ 200 nm) whereas covered films exhibit a larger W of ~130 meV that does not significantly depend on t (Figure 8a). The observed increase

in W with t in uncovered films indicates that W is smaller for circulites than for the underlayer. Indeed, the thinner the film, the larger the proportion of circulites (since the circulite layer is known to have fixed thickness of at most 20 nm) which implies that W is smaller for the circulites than for the underlayer morphology. Furthermore, because the W of covered films is larger than that of uncovered films, the W must also be smaller for circulites than for BOs.

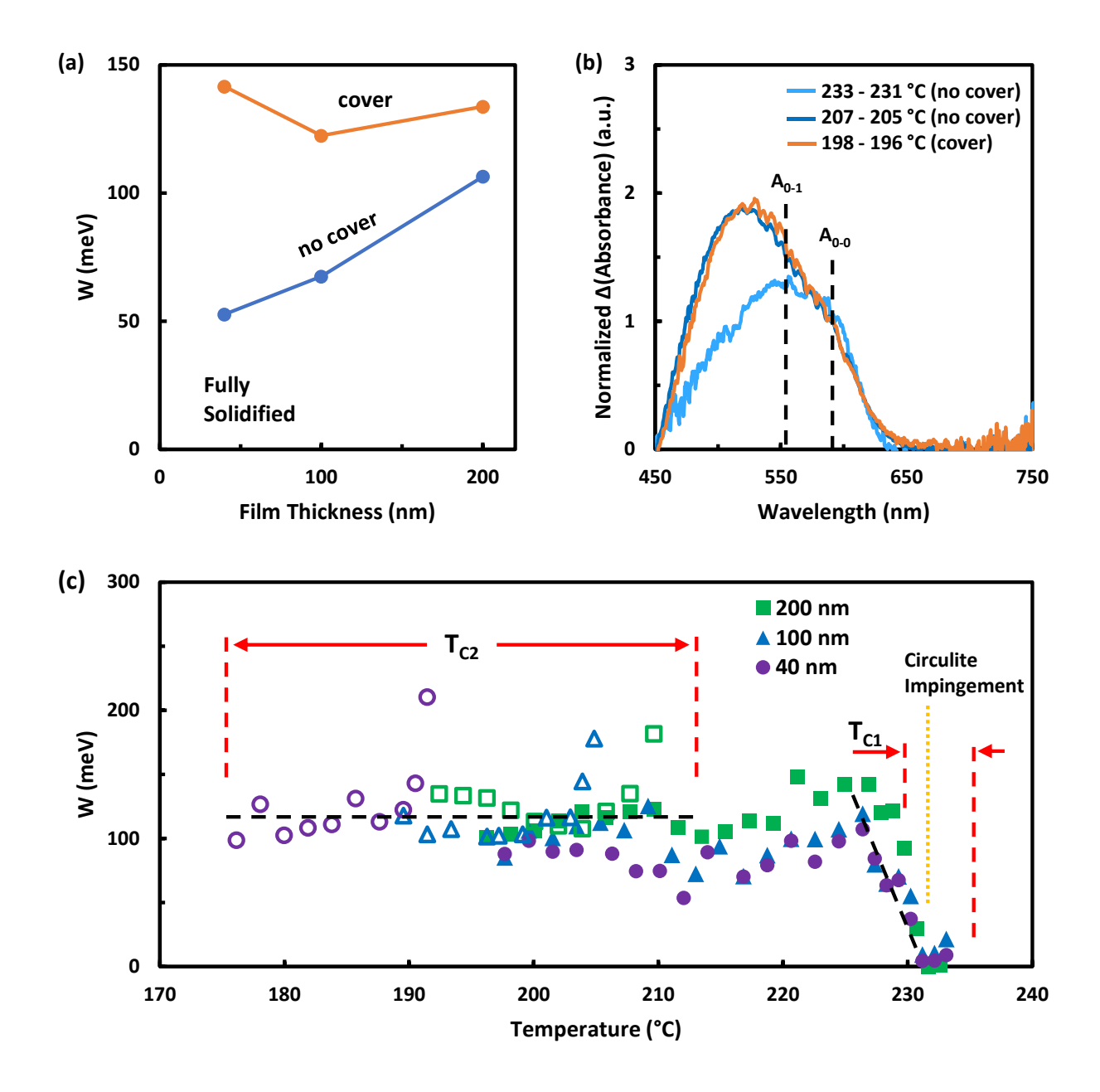


Figure 8. (a) Free exciton bandwidth W of fully solidified films. (b) Representative Δ (Absorbance) (difference in in-situ spectra 2 °C apart) normalized to the A_{0-0} peak during crystallization of uncovered (233 – 231 °C, and 207 – 205 °C) and covered (198 – 196 °C) films. (c) W from fitting Δ (Absorbance) spectra during crystallization of covered (open symbols) and uncovered (closed symbols) films. Black dashed lines are guide lines.

To isolate the optical properties of individual morphologies and how they evolve throughout the crystallization process, spectra were acquired in-situ during the crystallization process and the difference between spectra acquired 2 °C apart (Δ (Absorbance)) was computed. For example, the Δ (Absorbance) at 232 °C was calculated by subtracting the 233 °C absorbance spectrum from the 231 °C spectrum (Figure 8b), and therefore represents the optical absorption characteristics of only the crystallites that formed when cooling between 233 °C and 231 °C. Representative normalized Δ (Absorbance) spectra of circulites (233 - 231 °C, uncovered film), underlayer (207 - 205 °C, uncovered film), and BOs (198 - 196 °C, covered film) allow qualitative comparison of the $\Delta_{0-0}/\Delta_{0-1}$ ratio of each morphology: Figure 8b shows that circulite growth exhibits a large $\Delta_{0-0}/\Delta_{0-1}$ ratio (~0.91) whereas growth of bulk objects and the underlayer both have much smaller ratios (0.60 and 0.65 respectively). Note that subtraction of spectra at different temperatures not only allows the separation of the optical signatures of circulites and underlayer, but also facilitates fitting of high temperature spectra: for thicker films, the spectra acquired during circulite formation contain a large amorphous contribution from molten material which obscures the $\Delta_{0-0}/\Delta_{0-1}$ ratio (see UV-vis spectra for 229 °C in Figure S4a).

The fits of in-situ Δ (Absorbance) spectra reveal that the first circulites to form have an extremely small exciton bandwidth on the order of 1-10 meV (Figure 8c), which should correlate with extremely large conjugation lengths. Interestingly, the W of free surface-induced crystallites remains extremely small until the circulites impinge at ~231 °C (Figure S5), at which point W begins a sharp increase to ~130 meV at 227 °C suggesting that surface crystallites that form after circulite impingement have progressively smaller conjugation length with decreasing temperatures. In contrast, BO and underlayer growth corresponds to W ~ 110 meV throughout the crystallization process. Thus, the conjugation length of the first free-surface induced crystallites in the circulite layer is much longer than that of BOs and the underlayer.

3.5. Bulk vs. underlayer nucleation density

Considering that bulk objects and the underlayer differ slightly in T_C (~199 °C vs. ~205 °C) and considerably in morphological characteristics (isotropic individual resolvable objects vs. edge-on featureless morphology), the question arises about whether the observed differences result mainly from their nucleation behavior. It was previously inferred that the edge-on circulite layer nucleated edge-on oriented underlayer crystallites,²⁰ and it is feasible that such surface nucleation occurs with very high density resulting in an increase of T_C and optically unresolvable structures. To assess whether increasing the nucleation density of BOs results in crystallization temperatures that approach that of the underlayer, a self-nucleation (SN) thermal protocol⁵¹ was employed in covered and uncovered 200 nm films.

Upon SN of 200 nm covered films, the crystallization temperature T_c of BOs increases with decreasing self-nucleation temperature (T_s) and attains a maximum $T_{C,MAX}$ ~208 °C, similar to the underlayer T_c ~205 °C (Figure 9a and b). At the same time, the nucleation density increases dramatically until individual nucleation events are no longer distinguishable at T_s = 245 °C (Figure 9c)—qualitatively analogous to the underlayer (Figure 1). These results support the idea that nucleation density is one key difference between crystallization of the underlayer and of bulk objects. It is worth noting that the slightly higher value of $T_{C,MAX}$ for BOs vs. Tc of the underlayer (~208 °C vs 205 °C) may be explained by location of nucleation events: SN is expected to promote nucleation throughout the available volume whereas the underlayer nucleates only at one surface. Indeed, upon applying the SN protocol to a 200 nm uncovered film, the crystallization temperature of the underlayer of uncovered films slightly increases to the same $T_{C,MAX}$ ~ 208 °C as for BOs (Figure 9b squares) suggesting that the underlayer and BO crystallization behaviors are not fundamentally different; rather, they simply differ in that underlayer crystallizes nucleate with high density and edge-on orientation whereas BOs nucleate with relatively low density and random orientation. It is worth noting that the $T_{C,MAX}$ ~ 208 °C and maximum increase in crystallization temperature

 ΔT_{C} ~9.5 °C observed in thin films are comparable to those measured with DSC for a bulk sample of the same P3HT grade ($T_{C,MAX}$ ~ 205 °C and ΔT_{C} ~10 °C).¹

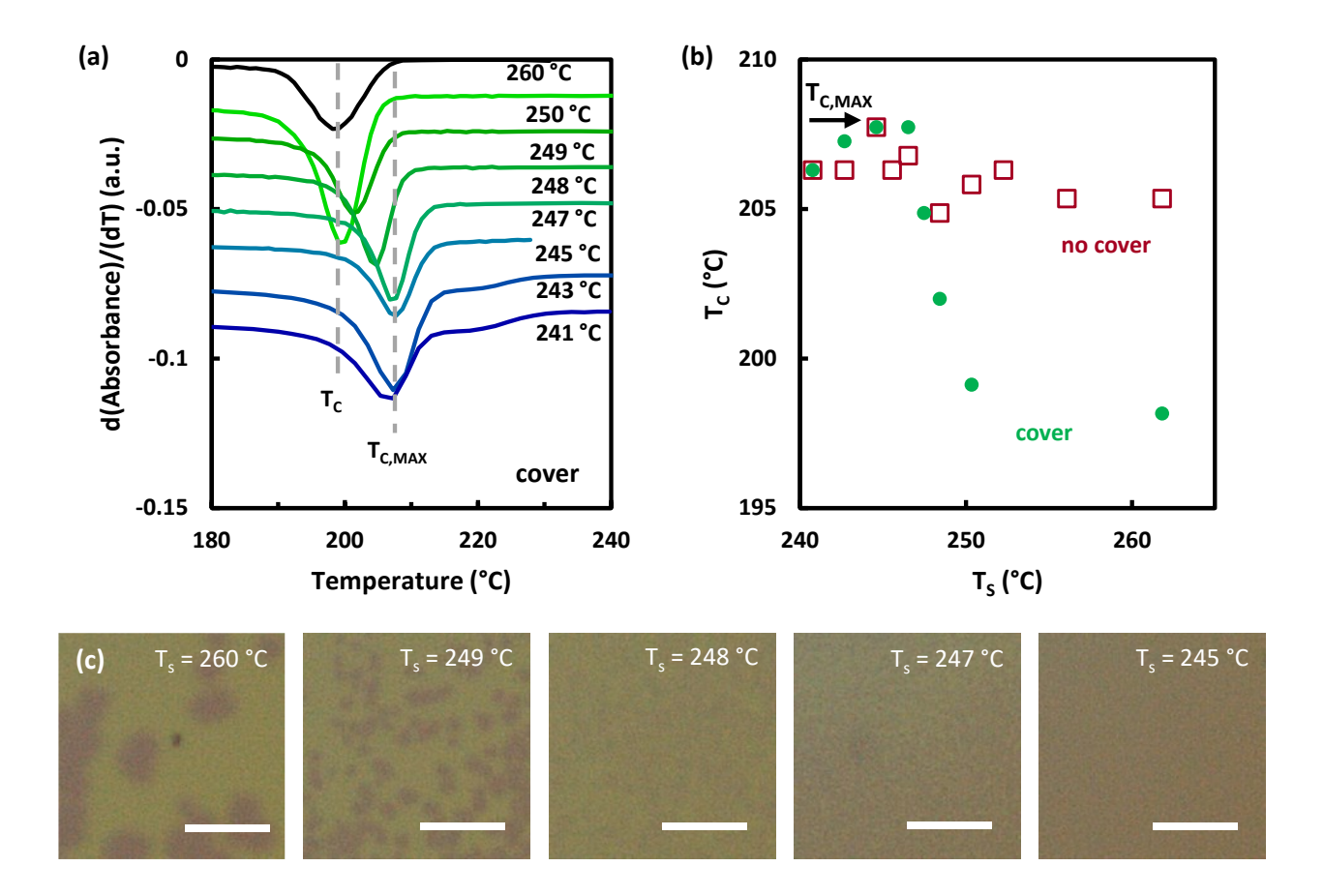


Figure 9. (a) Absorbance derivatives during crystallization after applying the SN thermal protocol to a ~200 nm covered film. (b) T_C vs. self-nucleation temperature (T_S) in 200 nm covered (circles) and uncovered (squares) films. (c) Representative transmission optical micrographs of a covered 200 nm film during crystallization after SN at T_S . Scalebar is 30 μ m.

4. Discussion

Here, three distinct types of morphologies—all of which correspond to form I crystal structure—were directly observed during melt-crystallization of P3HT thin films. Covered thin films (i.e. where no free

surface is available) develop the same type of morphology as bulk samples that are 10 µm thick: "bulk objects" or "BOs" which are highly absorbing, three-dimensional structures that crystallize with relatively low nucleation density. In contrast, uncovered thin films (i.e. with an air-polymer interface) develop "circulites"—i.e. two-dimensional spherulites confined within ~20 nm of the free surface—25 °C above bulk crystallization temperature, while the underlayer beneath the circulites develops featureless growth slightly above bulk crystallization temperatures. Interestingly, the surface circulites exhibit significantly increased linear growth rate compared to the bulk objects despite their higher T_C, providing new insight about the way surface freezing impacts the crystallization process. In addition, it is demonstrated that bulk objects can be formed even in very thin films (e.g. 40 nm) and do not exhibit any preferential crystalline orientation in the film. Given that the detailed semicrystalline morphology greatly impacts electronic properties, it follows that the presence or absence of a free surface has potential to be used to select optimal morphological characteristics of thin film active layers for specific applications.

The observation that free surface-induced circulites grow at least 1 order of magnitude faster than bulk objects (10-100 μ m/min vs. 1 μ m/min) is surprising, given that circulites develop at much higher temperatures (~238 °C vs. ~208 °C). Enhanced growth rates G at the air interface have been reported in small molecules when crystallized from the glassy state and have been attributed to high surface mobility. ⁵²⁻⁵⁵ However, such an explanation is unlikely for P3HT films. Both circulites and BOs have growth rates that increase with decreasing T_c , implying that their G is dominated by the thermodynamic driving force—not chain mobility. In other words, crystallization of both circulites and BOs corresponds to the right hand side of the typical bell-shaped G vs. T_c curve, as expected for crystallization temperatures that are closer to the melting point than to the glass transition, ⁵⁶⁻⁵⁷ and it is unlikely that the increased circulite G arises from greater chain mobility at the surface. Furthermore, the enhanced surface dynamics at the free surface observed in polymers such as polystyrene have been shown to only persist at temperatures near the $T_e^{26-28.58}$ and therefore, should not impact crystallization that occurs closer to the melting point.

Moreover, higher chain mobility at the free surface cannot be assumed: for example, thin films of some star polymers exhibit reduced surface relaxation dynamics compared to the bulk.⁵⁹ It is unclear whether P3HT would exhibit increased or decreased surface mobility, as the T_g of P3HT surface vs. bulk has not been reported. T_g of P3HT is notoriously difficult to measure⁶⁰⁻⁶² and differentiating the surface and bulk T_g would pose significant experimental challenges. However, surface and bulk T_g have been extracted for APFO3 and APFO-green9, both of which have chemical structures similar to P3HT—i.e. conjugated ring backbones and long alkyl side chains. Unlike polystyrene, these conjugated polymers exhibited higher T_g at the air-polymer interface than in the bulk, which implies lower chain mobility at the free surface than in the bulk.⁶³

Because the enhanced surface growth rate in P3HT cannot be explained by molecular mobility, another mechanism must be at play. A possible explanation could be that a molecular ordering event occurs at the free surface before or concomitantly with crystallization of circulites which results in an increase in crystalline growth rate. Although no evidence for a surface preordering event before circulite crystallization—such as a liquid crystalline phase—was experimentally detected, it cannot be discounted. Enhanced growth rates in classical semicrystalline polymers have been measured for crystallization that occurs while flow is imposed and have been attributed to a flow-induced molecular pre-orientation. Face surface-induced preordering of P3HT molecules could feasibly enhance the circulite growth rate. If a nucleation constant analysis is performed using an equilibrium melting temperature of 257 °C (estimated for infinite Mw and 95% regioregularity), for then the nucleation constant Kg for BOs is at least 3.6 times larger than that of circulites (Table S1), suggesting that the surface free energy product for circulites is smaller than for BOs. A possible cause for a reduced surface free energy product is increased chain extension, keeping which could occur due to pre-ordering at the air-polymer interface. It has also been suggested that preordering can enhance nucleation in other materials, possibly through

a reduction in the required energy barrier,⁶⁹⁻⁷⁰ but the primary nucleation density of circulites was not observed to be higher than that in the bulk.

Interestingly, the maximum observed melting temperature $T_{M,END}$ of circulites (264.5 °C, Figure S7) is well above the predicted equilibrium melting temperature of 251.5 °C for M_W = 40 kg/mol and RR = 95%, and even above the predicted melting temperature of 257 °C for infinite M_W 95% regioregular chains. ⁶⁶ This could be due to a transition into a non-equilibrium disentangled melt state at the surface ⁷¹ or to a reduction in entropy due to a transition into a phase with intermediate degree of ordering—such as a liquid-crystalline phase. Interestingly, a nematic phase has been predicted for P3HT near the melting point; ⁷² however, the predicted melting and nematic-to-isotropic temperatures are close together, ⁶⁶ which might make detecting a nematic phase difficult.

Analysis of ex-situ UV-vis spectra suggests that the free exciton bandwidth (W)—thought to be a key parameter for organic electronic device performance—can be manipulated through film thickness and the presence or absence of a free surface during melt-crystallization because circulites make up a much larger fraction of thinner films and form with much smaller W than bulk objects and the underlayer. It is generally assumed that crystallization at higher temperatures results in thicker lamellae⁷³ which, in turn, have been correlated with increased conjugation length.^{34, 74-75} Because the conjugation length and W are inversely related, ^{38, 41, 50} the smaller W of circulites is consistent with being formed at significantly higher temperatures compared to the BOs. Although electronic performance does not depend exclusively on conjugation length—e.g. orientation and crystalline connectivity are also critical factors—the extremely low W of the first circulite crystals suggests that they have the potential to exhibit excellent charge mobility.

Remarkably, isotropic crystallization was achieved in P3HT thin films even as thin as 40 nm by coating the film with aluminum and thus removing the free surface of the film. P3HT films typically exhibit edge-

on orientation⁷⁶⁻⁷⁸ which in some studies was attributed to a SiO₂ substrate-induced effect; however, no such effect was observed here. Indeed, the covered films exhibit isotropic crystallization. Edge-on orientation is only obtained in uncovered films and attributed to the presence of a free surface during melt-crystallization. Note that the observed edge-on scattering from uncovered films arises not only from the highly oriented surface frozen layer but also from the underlayer;²⁰ in other words, the presence of a free surface affects crystalline orientation beyond the 20 top nm of the film. Preferential orientation has also been reported in thin films of classical semicrystalline polymers for film thicknesses below ~200 nm and attributed to the inability of lamellae to freely rotate due to confinement effects;^{16,79-81} however, such confinement effects are not observed here even for covered 40 nm P3HT films. There are other examples of ultrathin films where a lack of orientation in ultrathin films has been reported: in linear low density polyethylene, confined flat-on oriented lamellae do not appear until the film thickness decreased below 30 nm—on the order of a single lamellar thickness.⁸² Finally, it is possible that the reduced G measured for bulk objects in covered 40 nm P3HT films arises from substrate and top cover interactions: in literature, reduced growth rates in classical polymer thin films have been attributed to substrate interactions that decrease molecular mobility.^{12-13,83}

Conclusions

Here, we show that the presence or absence of an air-polymer interface can be used to manipulate the crystallization process, final semicrystalline morphology, and molecular orientation in P3HT thin films. By covering a thin film so that no free surface is available, bulk crystallization morphology is attained: highly absorbing "bulk objects" grow throughout the film thickness near the bulk crystallization temperature ($T_{C,BULK}$) with isotropic orientation. In contrast, in uncovered thin films, highly edge-on oriented 2D spherulites ("circulites") crystallize within the top 20 nm of the film at temperatures ~25 °C higher than $T_{C,BULK}$ and, upon reaching ~5 °C > $T_{C,BULK}$, the circulite layer induces edge-on oriented,

featureless crystallization in the underlayer. In addition to affecting the molecular orientation, the presence of an air interface is shown to increase the conjugation length for thin films compared to when no free surface is available. Furthermore, the surface circulites and the bulk objects crystalline growth rates G were measured for the first time and their comparison provides insight on the impact of an air-polymer interface on the melt-crystallization process. Although T_{C,CIRCULITES} >> T_{C,BOS}, circulites exhibit growth rates ~10x faster than the bulk objects. Chain mobility is unlikely to cause the circulite enhanced G since both circulites and bulk objects crystallize close to the melting point, where chain mobility is not expected to dominate the temperature dependence of growth rates. The observed difference in linear growth rates can also not be ascribed to crystal structure—given that both circulites and bulk objects exhibit form I crystal structure—so another mechanism must be at play such as a free surface-induced preorientation event that increases G at the air-polymer interface. Because there is a complex interplay between orientation, mesoscale morphology, and conjugation length which dictate performance of electronic devices, the presence or absence of an air-polymer interface during melt crystallization of polymer films has potential as a processing parameter to manipulate final morphology and properties of active layers.

Associated content

Supporting Information - Optical micrographs, I vs. q X-ray data, and UV-vis spectra.

Author information

Corresponding Author

Lucia Fernandez-Ballester – Department of Mechanical and Materials Engineering and Nebraska Center for Materials and Nanoscience, University of Nebraska at Lincoln, Lincoln, Nebraska 68588, United States; orcid.org/0000-0001-6956-5104; Email: lucia.fernandez@unl.edu

Authors

Jesse Kuebler – Department of Mechanical and Materials Engineering and Nebraska Center for Materials and Nanoscience, University of Nebraska at Lincoln, Lincoln, Nebraska 68588, United States

Sunil Dhapola – Department of Mechanical and Materials Engineering and Nebraska Center for Materials and Nanoscience, University of Nebraska at Lincoln, Lincoln, Nebraska 68588, United States

Notes

The authors declare no competing financial interest.

Acknowledgements

The authors gratefully acknowledge funding of this work by the National Science Foundation under award DMR-1809888. This research used resources of the Advanced Photon Source, a U.S. Department of Energy (DOE) Office of Science user facility operated for the DOE Office of Science by Argonne National Laboratory under Contract No. DE-AC02-06CH11357. Profilometry was performed at the NanoEngineering Research Core Facility (NERCF), which is partially funded by the Nebraska Research Initiative. We are grateful to Joseph Strzalka and Xiaobing Zuo for assistance during X-ray experiments.

References

- 1. Hosseinabad, R.; Kuebler, J.; Fernandez-Ballester, L., Combined role of regioregularity and molecular weight on melt-crystallization and self-nucleation of poly (3-hexylthiophene). *Polymer* **2022**, *259*, 125341.
- 2. Bao, Z.; Dodabalapur, A.; Lovinger, A. J., Soluble and processable regioregular poly (3-hexylthiophene) for thin film field-effect transistor applications with high mobility. *Applied physics letters* **1996**, *69* (26), 4108-4110.

- 3. Li, G.; Shrotriya, V.; Huang, J.; Yao, Y.; Moriarty, T.; Emery, K.; Yang, Y., High-efficiency solution processable polymer photovoltaic cells by self-organization of polymer blends. *Nature Materials* **2005**, *4* (11), 864-868.
- 4. Chang, J.-F.; Sun, B.; Breiby, D. W.; Nielsen, M. M.; Sölling, T. I.; Giles, M.; McCulloch, I.; Sirringhaus, H., Enhanced mobility of poly (3-hexylthiophene) transistors by spin-coating from high-boiling-point solvents. *Chemistry of Materials* **2004**, *16* (23), 4772-4776.
- 5. Müller, C.; Zhigadlo, N. D.; Kumar, A.; Baklar, M. A.; Karpinski, J.; Smith, P.; Kreouzis, T.; Stingelin, N., Enhanced charge-carrier mobility in high-pressure-crystallized poly (3-hexylthiophene).

 Macromolecules 2011, 44 (6), 1221-1225.
- 6. Noriega, R.; Rivnay, J.; Vandewal, K.; Koch, F. P.; Stingelin, N.; Smith, P.; Toney, M. F.; Salleo, A., A general relationship between disorder, aggregation and charge transport in conjugated polymers.

 Nature materials 2013, 12 (11), 1038-1044.
- 7. O'Connor, B.; Kline, R. J.; Conrad, B. R.; Richter, L. J.; Gundlach, D.; Toney, M. F.; DeLongchamp, D. M., Anisotropic Structure and Charge Transport in Highly Strain-Aligned Regioregular Poly (3-hexylthiophene). *Advanced Functional Materials* **2011**, *21* (19), 3697-3705.
- 8. Gu, K.; Snyder, C. R.; Onorato, J.; Luscombe, C. K.; Bosse, A. W.; Loo, Y.-L., Assessing the huang–brown description of tie chains for charge transport in conjugated polymers. *ACS Macro Letters* **2018**, *7* (11), 1333-1338.
- 9. Schulz, G. L.; Ludwigs, S., Controlled crystallization of conjugated polymer films from solution and solvent vapor for polymer electronics. *Advanced Functional Materials* **2017**, *27* (1), 1603083.
- 10. Michell, R. M.; Mueller, A. J., Confined crystallization of polymeric materials. *Progress in Polymer Science* **2016**, *54*, 183-213.

- 11. Napolitano, S.; Wübbenhorst, M., Deviation from bulk behaviour in the cold crystallization kinetics of ultrathin films of poly (3-hydroxybutyrate). *Journal of Physics: Condensed Matter* **2007**, *19* (20), 205121.
- 12. Napolitano, S.; Wübbenhorst, M., Effect of a reduced mobility layer on the interplay between molecular relaxations and diffusion-limited crystallization rate in ultrathin polymer films. *The Journal of Physical Chemistry B* **2007**, *111* (21), 5775-5780.
- 13. Schönherr, H.; Frank, C. W., Ultrathin films of poly (ethylene oxides) on oxidized silicon. 2. In situ study of crystallization and melting by hot stage AFM. *Macromolecules* **2003**, *36* (4), 1199-1208.
- 14. Cho, K.; Kim, D.; Yoon, S., Effect of substrate surface energy on transcrystalline growth and its effect on interfacial adhesion of semicrystalline polymers. *Macromolecules* **2003**, *36* (20), 7652-7660.
- 15. Reiter, G.; Sommer, J.-U., Crystallization of adsorbed polymer monolayers. *Physical review letters* **1998**, *80* (17), 3771.
- 16. Liu, Y.-X.; Chen, E.-Q., Polymer crystallization of ultrathin films on solid substrates. *Coordination Chemistry Reviews* **2010**, *254* (9-10), 1011-1037.
- 17. Massa, M. V.; Dalnoki-Veress, K.; Forrest, J., Crystallization kinetics and crystal morphology in thin poly (ethylene oxide) films. *The European Physical Journal E* **2003**, *11*, 191-198.
- 18. Bertoldo, M.; Labardi, M.; Rotella, C.; Capaccioli, S., Enhanced crystallization kinetics in poly (ethylene terephthalate) thin films evidenced by infrared spectroscopy. *Polymer* **2010**, *51* (16), 3660-3668.
- 19. Yang, Y.; Tian, H.; Napolitano, S.; Zuo, B., Crystallization in thin films of polymer glasses: The role of free surfaces, solid interfaces and their competition. *Progress in Polymer Science* **2023**, 101725.
- 20. Kuebler, J.; Loosbrock, T.; Strzalka, J.; Fernandez-Ballester, L., Direct Observation of Two-Step, Stratified Crystallization and Morphology in Conjugated Polymer Thin Films. *Macromolecules* **2023**, *56* (8), 3083-3094.

- 21. Ocko, B.; Wu, X.; Sirota, E.; Sinha, S.; Gang, O.; Deutsch, M., Surface freezing in chain molecules: Normal alkanes. *Physical Review E* **1997**, *55* (3), 3164.
- 22. Cholakova, D.; Denkov, N., Rotator phases in alkane systems: In bulk, surface layers and micro/nano-confinements. *Advances in colloid and interface science* **2019**, *269*, 7-42.
- 23. Prasad, S.; Jiang, Z.; Sinha, S. K.; Dhinojwala, A., Partial crystallinity in alkyl side chain polymers dictates surface freezing. *Physical review letters* **2008**, *101* (6), 065505.
- 24. Dolynchuk, O.; Schmode, P.; Fischer, M.; Thelakkat, M.; Thurn-Albrecht, T., Elucidating the Effect of Interfacial Interactions on Crystal Orientations in Thin Films of Polythiophenes. *Macromolecules* **2021**, *54* (12), 5429-5439.
- 25. Balko, J.; Portale, G.; Lohwasser, R. H.; Thelakkat, M.; Thurn-Albrecht, T., Surface induced orientation and vertically layered morphology in thin films of poly (3-hexylthiophene) crystallized from the melt. *Journal of Materials Research* **2017**, *32* (10), 1957-1968.
- 26. Ellison, C. J.; Torkelson, J. M., The distribution of glass-transition temperatures in nanoscopically confined glass formers. *Nature materials* **2003**, *2* (10), 695-700.
- 27. Zuo, B.; Xu, J.; Sun, S.; Liu, Y.; Yang, J.; Zhang, L.; Wang, X., Stepwise crystallization and the layered distribution in crystallization kinetics of ultra-thin poly (ethylene terephthalate) film. *The Journal of Chemical Physics* **2016**, *144* (23), 234902.
- 28. Xu, Q.; Zhu, N.; Fang, H.; Wang, X.; Priestley, R. D.; Zuo, B., Decoupling role of film thickness and interfacial effect on polymer thin film dynamics. *ACS Macro Letters* **2020**, *10* (1), 1-8.
- 29. Frenken, J. W.; Van der Veen, J., Observation of surface melting. *Physical review letters* **1985**, *54* (2), 134.
- 30. Elbaum, M.; Schick, M., Application of the theory of dispersion forces to the surface melting of ice. *Physical review letters* **1991**, *66* (13), 1713.

- 31. Gang, O.; Wu, X.; Ocko, B.; Sirota, E.; Deutsch, M., Surface freezing in chain molecules. II. Neat and hydrated alcohols. *Physical Review E* **1998**, *58* (5), 6086.
- 32. Gautam, K.; Dhinojwala, A., Melting at alkyl side chain comb polymer interfaces. *Physical review letters* **2002**, *88* (14), 145501.
- 33. Koch, F. P. V.; Heeney, M.; Smith, P., Thermal and structural characteristics of oligo (3-hexylthiophene) s (3HT) n, n= 4–36. *Journal of the American Chemical Society* **2013**, *135* (37), 13699-13709.
- 34. Crossland, E. J.; Rahimi, K.; Reiter, G.; Steiner, U.; Ludwigs, S., Systematic Control of Nucleation Density in Poly (3-Hexylthiophene) Thin Films. *Advanced Functional Materials* **2011**, *21* (3), 518-524.
- 35. AlShetwi, Y. A.; Bessif, B.; Sommer, M.; Reiter, G. n., Illumination of Conjugated Polymers

 Reduces the Nucleation Probability and Slows Down the Crystal Growth Rate. *Macromolecules* **2021,** *54*(24), 11478-11485.
- 36. Malik, S.; Nandi, A. K., Crystallization mechanism of regioregular poly(3-alkyl thiophene)s. Journal of Polymer Science Part B: Polymer Physics **2002**, 40 (18), 2073-2085.
- 37. Maiz, J.; Liu, G.; Ruiperez, F.; Delbosc, N.; Coulembier, O.; Wang, D.; Müller, A. J., How cyclic chain topology can reduce the crystallization rate of poly (3-hexylthiophene) and promote the formation of liquid crystalline phases in comparison with linear analogue chains. *Journal of Materials Chemistry C* **2019,** *7* (22), 6548-6558.
- 38. Brinkmann, M.; Rannou, P., Molecular weight dependence of chain packing and semicrystalline structure in oriented films of regioregular poly (3-hexylthiophene) revealed by high-resolution transmission electron microscopy. *Macromolecules* **2009**, *42* (4), 1125-1130.
- 39. Mena-Osteritz, E.; Meyer, A.; Langeveld-Voss, B. M.; Janssen, R. A.; Meijer, E.; Bäuerle, P., Two-dimensional crystals of poly (3-alkyl-thiophene) s: direct visualization of polymer folds in submolecular resolution. *Angewandte Chemie International Edition* **2000**, *39* (15), 2679-2684.

- 40. Spano, F. C., Modeling disorder in polymer aggregates: The optical spectroscopy of regionegular poly (3-hexylthiophene) thin films. *The Journal of chemical physics* **2005**, *122* (23), 234701.
- 41. Spano, F. C., Absorption in regio-regular poly (3-hexyl) thiophene thin films: Fermi resonances, interband coupling and disorder. *Chemical physics* **2006**, *325* (1), 22-35.
- 42. Schneider, C. A.; Rasband, W. S.; Eliceiri, K. W., NIH Image to ImageJ: 25 years of image analysis. *Nature methods* **2012**, *9* (7), 671-675.
- Jiang, Z.; Li, X.; Strzalka, J.; Sprung, M.; Sun, T.; Sandy, A. R.; Narayanan, S.; Lee, D. R.; Wang, J., The dedicated high-resolution grazing-incidence X-ray scattering beamline 8-ID-E at the Advanced Photon Source. *Journal of synchrotron radiation* **2012**, *19* (4), 627-636.
- 44. Jiang, Z., GIXSGUI: a MATLAB toolbox for grazing-incidence X-ray scattering data visualization and reduction, and indexing of buried three-dimensional periodic nanostructured films. *Journal of Applied Crystallography* **2015**, *48* (3), 917-926.
- 45. Tolan, M.; Tolan, M., *X-ray scattering from soft-matter thin films: materials science and basic research*. Springer: 1999; Vol. 148.
- 46. Liu, J.; Sun, Y.; Gao, X.; Xing, R.; Zheng, L.; Wu, S.; Geng, Y.; Han, Y., Oriented poly (3-hexylthiophene) Nanofibril with the π π stacking growth direction by solvent directional evaporation. *Langmuir* **2011**, *27* (7), 4212-4219.
- 47. Meille, S. V.; Romita, V.; Caronna, T.; Lovinger, A. J.; Catellani, M.; Belobrzeckaja, L., Influence of molecular weight and regioregularity on the polymorphic behavior of poly (3-decylthiophenes).

 Macromolecules 1997, 30 (25), 7898-7905.
- 48. Joshi, S.; Grigorian, S.; Pietsch, U., X-ray structural and crystallinity studies of low and high molecular weight poly (3-hexylthiophene). *Physica status solidi (a)* **2008**, *205* (3), 488-496.

- 49. Rahimi, K.; Botiz, I.; Stingelin, N.; Kayunkid, N.; Sommer, M.; Koch, F. P. V.; Nguyen, H.; Coulembier, O.; Dubois, P.; Brinkmann, M., Controllable processes for generating large single crystals of poly (3-hexylthiophene). *Angewandte Chemie* **2012**, *124* (44), 11293-11297.
- 50. Gierschner, J.; Huang, Y.-S.; Van Averbeke, B.; Cornil, J.; Friend, R. H.; Beljonne, D., Excitonic versus electronic couplings in molecular assemblies: The importance of non-nearest neighbor interactions. *The Journal of chemical physics* **2009**, *130* (4), 044105.
- 51. Fillon, B.; Wittmann, J. C.; Lotz, B.; Thierry, A., Self-nucleation and recrystallization of isotactic polypropylene (α phase) investigated by differential scanning calorimetry. *Journal of Polymer Science*Part B: Polymer Physics **1993**, *31* (10), 1383-1393.
- 52. Huang, C.; Ruan, S.; Cai, T.; Yu, L., Fast surface diffusion and crystallization of amorphous griseofulvin. *The Journal of Physical Chemistry B* **2017**, *121* (40), 9463-9468.
- 53. Wu, T.; Yu, L., Surface crystallization of indomethacin below T g. *Pharmaceutical research* **2006**, 23, 2350-2355.
- 54. Zhu, L.; Wong, L.; Yu, L., Surface-enhanced crystallization of amorphous nifedipine. *Molecular pharmaceutics* **2008**, *5* (6), 921-926.
- 55. Yu, L., Surface mobility of molecular glasses and its importance in physical stability. *Advanced drug delivery reviews* **2016**, *100*, 3-9.
- 56. Lauritzen Jr, J. I.; Hoffman, J. D., Extension of theory of growth of chain-folded polymer crystals to large undercoolings. *Journal of applied Physics* **1973**, *44* (10), 4340-4352.
- 57. Sperling, L. H., *Introduction to physical polymer science*. John Wiley & Sons: 2005.
- 58. Paeng, K.; Swallen, S. F.; Ediger, M., Direct measurement of molecular motion in freestanding polystyrene thin films. *Journal of the American Chemical Society* **2011**, *133* (22), 8444-8447.
- 59. Glynos, E.; Johnson, K. J.; Frieberg, B.; Chremos, A.; Narayanan, S.; Sakellariou, G.; Green, P. F., Free surface relaxations of star-shaped polymer films. *Physical review letters* **2017**, *119* (22), 227801.

- 60. Hopkinson, P. E.; Staniec, P. A.; Pearson, A. J.; Dunbar, A. D.; Wang, T.; Ryan, A. J.; Jones, R. A.; Lidzey, D. G.; Donald, A. M., A phase diagram of the P3HT: PCBM organic photovoltaic system: implications for device processing and performance. *Macromolecules* **2011**, *44* (8), 2908-2917.
- Zhao, J.; Swinnen, A.; Van Assche, G.; Manca, J.; Vanderzande, D.; Mele, B. V., Phase diagram of P3HT/PCBM blends and its implication for the stability of morphology. *The Journal of Physical Chemistry B* **2009**, *113* (6), 1587-1591.
- 62. Zhao, Y.; Yuan, G.; Roche, P.; Leclerc, M., A calorimetric study of the phase transitions in poly (3-hexylthiophene). *Polymer* **1995**, *36* (11), 2211-2214.
- 63. Müller, C.; Andersson, L. M.; Peña-Rodríguez, O.; Garriga, M.; Inganäs, O.; Campoy-Quiles, M., Determination of thermal transition depth profiles in polymer semiconductor films with ellipsometry.

 Macromolecules 2013, 46 (18), 7325-7331.
- 64. Troisi, E.; Caelers, H.; Peters, G., Full characterization of multiphase, multimorphological kinetics in flow-induced crystallization of IPP at elevated pressure. *Macromolecules* **2017**, *50* (10), 3868-3882.
- 65. Pantani, R.; Coccorullo, I.; Volpe, V.; Titomanlio, G., Shear-induced nucleation and growth in isotactic polypropylene. *Macromolecules* **2010**, *43* (21), 9030-9038.
- 66. Snyder, C. R.; Gomez, E. D., Phase behavior of poly (3-hexylthiophene-2, 5-diyl). *Journal of Polymer Science Part B: Polymer Physics* **2016**, *54* (13), 1202-1206.
- 67. Hoffman, J. D.; Miller, R. L., Kinetic of crystallization from the melt and chain folding in polyethylene fractions revisited: theory and experiment. *Polymer* **1997**, *38* (13), 3151-3212.
- 68. Hoffman, J. D.; Miller, R. L.; Marand, H.; Roitman, D. B., Relationship between the lateral surface free energy. sigma. and the chain structure of melt-crystallized polymers. *Macromolecules* **1992**, *25* (8), 2221-2229.

- 69. Pirela, V.; Campoy-Quiles, M.; Müller, A. J.; Martín, J., Unraveling the Influence of the Preexisting Molecular Order on the Crystallization of Semiconducting Semicrystalline Poly (9, 9-di-n-octylfluorenyl-2, 7-diyl (PFO). *Chemistry of Materials* **2022**, *34* (23), 10744-10751.
- 70. Wu, H.; Yao, X.; Gui, Y.; Hao, H.; Yu, L., Surface enhancement of crystal nucleation in amorphous acetaminophen. *Crystal Growth & Design* **2022**, *22* (9), 5598-5606.
- 71. Lippits, D. R.; Rastogi, S.; Höhne, G. W.; Mezari, B.; Magusin, P. C., Heterogeneous distribution of entanglements in the polymer melt and its influence on crystallization. *Macromolecules* **2007**, *40* (4), 1004-1010.
- 72. Zhang, W.; Gomez, E. D.; Milner, S. T., Surface-induced chain alignment of semiflexible polymers. *Macromolecules* **2016**, *49* (3), 963-971.
- 73. Hoffman, J. D.; Weeks, J. J., Melting process and the equilibrium melting temperature of polychlorotrifluoroethylene. *J. Res. Natl. Bur. Stand., Sect. A* **1962**, *66* (1), 13-28.
- 74. Turner, S. T.; Pingel, P.; Steyrleuthner, R.; Crossland, E. J.; Ludwigs, S.; Neher, D., Quantitative analysis of bulk heterojunction films using linear absorption spectroscopy and solar cell performance. *Advanced Functional Materials* **2011**, *21* (24), 4640-4652.
- 75. Hamidi-Sakr, A.; Biniek, L.; Fall, S.; Brinkmann, M., Precise Control of Lamellar Thickness in Highly Oriented Regioregular Poly (3-Hexylthiophene) Thin Films Prepared by High-Temperature Rubbing: Correlations with Optical Properties and Charge Transport. *Advanced Functional Materials* **2016**, *26* (3), 408-420.
- 76. Jimison, L. H.; Himmelberger, S.; Duong, D. T.; Rivnay, J.; Toney, M. F.; Salleo, A., Vertical confinement and interface effects on the microstructure and charge transport of P3HT thin films. *Journal of Polymer Science Part B: Polymer Physics* **2013**, *51* (7), 611-620.
- 77. Joseph Kline, R.; McGehee, M. D.; Toney, M. F., Highly oriented crystals at the buried interface in polythiophene thin-film transistors. *Nature Materials* **2006**, *5* (3), 222-228.

- 78. Verploegen, E.; Mondal, R.; Bettinger, C. J.; Sok, S.; Toney, M. F.; Bao, Z., Effects of thermal annealing upon the morphology of polymer–fullerene blends. *Advanced Functional Materials* **2010**, *20* (20), 3519-3529.
- 79. Jeon, K.; Krishnamoorti, R., Morphological behavior of thin linear low-density polyethylene films. *Macromolecules* **2008**, *41* (19), 7131-7140.
- 80. Schönherr, H.; Frank, C. W., Ultrathin films of poly (ethylene oxides) on oxidized silicon. 1. Spectroscopic characterization of film structure and crystallization kinetics. *Macromolecules* **2003**, *36* (4), 1188-1198.
- 81. Liang, Y.; Zheng, M.; Park, K. H.; Lee, H. S., Thickness-dependent crystal orientation in poly (trimethylene 2, 6-naphthalate) films studied with GIWAXD and RA-FTIR methods. *Polymer* **2008**, *49* (7), 1961-1967.
- Wang, Y.; Ge, S.; Rafailovich, M.; Sokolov, J.; Zou, Y.; Ade, H.; Lüning, J.; Lustiger, A.; Maron, G., Crystallization in the thin and ultrathin films of poly (ethylene– vinyl acetate) and linear low-density polyethylene. *Macromolecules* **2004**, *37* (9), 3319-3327.
- 83. Sawamura, S.; Miyaji, H.; Izumi, K.; Sutton, S. J.; Miyamoto, Y., Growth rate of isotactic polystyrene crystals in thin films. *Journal of the Physical Society of Japan* **1998**, *67* (10), 3338-3344.